Turkish Journal of Civil Engineering, 2026, 35-63, Paper 824, ***Research Article***

The Effect of Aspect Ratio on the Shape Factors of Rectangular Footings on Sandy Soil

Kaan YÜNKÜL[1]*
Ayhan GÜRBÜZ[2]
Sarper DEMİRDÖĞEN[3]

ABSTRACT

The dimensional of the footing is crucial parameter affecting the ultimate bearing capacity and failure surface geometry. However, the recommendations found in the literature often conflict with one another. Therefore, in this study, rigorous parametric three-dimensional finite element analyses using PLAXIS 3D with the Hardening Soil (*HS*) model were conducted to examine the unit weight component of the shape factors (S_γ), the pressure-settlement responses and the failure mechanisms of rectangular footings with an aspect ratio (*L/B*), defined as the ratio of the length (*L*) to the width (*B*) of the footing, ranging from 1 to 10. These analyses were performed four relative densities (D_r) of the sandy soil ranging from 10% to 80%. The results revealed that S_γ values increased with the *L/B* ratio, peaking at *L/B*=1.5, followed by a decline as the *L/B* ratio continued to increase. An increase in the internal friction angle of the soil led to higher S_γ values. This behavior contradicts some earlier studies and is attributed to the three-dimensional interaction of the failure surface, failure surface geometry and displaced soil volume. Furthermore, non-linear regression analysis was performed to produce novel equations to predict S_γ for rectangular footings and unit weight component of the bearing capacity factor (N_γ) for strip footings in sandy soil, demonstrating strong agreement with *FE* results.

Keywords: Shape factor, aspect ratio, shallow footing, finite element analysis, PLAXIS 3D.

Note:
- This paper was received on February 11, 2025 and accepted for publication by the Editorial Board on August 31, 2025.
- Discussions on this paper will be accepted by March 31, 2026.
- https://doi.org/10.18400/tjce.1637258

1 Tokat Gaziosmanpaşa University, Department of Civil Engineering, Tokat, Türkiye
kaan.yunkul@gop.edu.tr - https://orcid.org/0000-0003-1264-237X

2 Gazi University, Department of Civil Engineering, Ankara, Türkiye
agurbuz@gazi.edu.tr - https://orcid.org/0000-0002-0459-7129

3 The University of Kansas, Dep. of Civil, Environmental Architectural Engineering, Lawrence, USA
sarperdemirdogen@gmail.com - https://orcid.org/0000-0001-8576-0807

* Corresponding author

1. INTRODUCTION

The design of a shallow footing, which is a geotechnical structure that transfers the superstructure's load to the underlying soil, requires the evaluation of both settlement and ultimate bearing capacity. The traditional ultimate bearing capacity equation was first introduced by Terzaghi [1] for strip footings under plane strain conditions. This equation incorporates bearing capacity factors for cohesion (N_c), surcharge (N_q) and unit weight (N_γ), all of which depend on the soil's internal friction angle value. Several researchers have proposed different N_γ equations due to variations in the footing failure surface geometries although the equation proposed by Prandtl [2] for N_c value and the equation proposed by Reissner [3] for N_q value are widely accepted in the literature. The equations for the prediction of the N_γ values suggested by various researchers are summarized in Table 1. The proposed equation for strip footings is modified for rectangular footings by incorporating shape factors: cohesion component (S_c), surcharge component (S_q) and unit weight component (S_γ). The cohesion (c) and surcharge (q) values are zero when the shallow footing is placed on the ground surface and the underlying soil is cohesionless. In this situation, the ultimate bearing capacity is as in Equation (1) and S_γ value is determined as the ratio of ultimate bearing capacity of the rectangular footing to that of the ultimate bearing capacity of strip footing, as given in Equation (2).

Table 1 - Summary of the N_γ equations in the literature

Researchers	N_γ	**Researchers**	N_γ
Terzaghi [1]	$(N_q+3)\tan(1.34\phi)$	Hjiaj et al. [10]	$e^{\left[\frac{\pi}{6}(1+3\pi tan\phi\right]}(\tan\phi)^{2\pi/5}$
Meyerhof [4]	$(N_q-1)\tan(1.4\phi)$	Martin et al. [11]	$\left[N_q-1\right]\tan(1.338\phi)$
Hansen [5]	$1.5(N_q-1)\tan(\phi)$	Kumar and Kouzer [12]	$\left[1.012N_q-0.226\right]\tan(1.426\phi)$
Vesic [6]	$2(N_q+1)\tan(\phi)$	Lyamin et al. [13]	$\left[N_q-0.6\right]\tan(1.33\phi)$
Michalowski [7]	$e^{(0.66+5.11tan\phi)}\tan(\phi)$	Jahanandish et al. [14]	$\left[N_q+1\right]\tan(1.5\phi)$
Soubra [8]	$\left[1.374N_q-0.162\right]\tan(1.343\phi)$	Kumar and Khatri [15]	$\left[N_q-1\right]\tan(1.264\phi)$
Zhu [9]	$\left[2N_q+1\right](\tan\phi)^{1.35}$	TBEC [16]	$2(N_q-1)\tan(\phi)$

Note: $N_q=tan^2\left(45+\frac{\phi}{2}\right)e^{\pi tan\phi}$ [3], ϕ refers to the internal friction angle of the soil beneath the footing

$$q_{ult}=\frac{1}{2}B\gamma' N_\gamma S_\gamma \tag{1}$$

$$S_\gamma=\frac{q_{ult(r)}}{q_{ult(s)}} \tag{2}$$

where q_{ult} is the ultimate bearing capacity of a surface footing, that is, a shallow footing placed on ground surface, on cohesionless soil, B is the width of the footing, γ' is the effective unit weight of the soil under the footing, N_γ is the unit weight component of the bearing capacity, S_γ is unit weight component of the shape factor, $q_{ult(r)}$ is the ultimate bearing

capacity of the rectangular surface footing on cohesionless soil, $q_{ult(s)}$ is the ultimate bearing capacity of the strip surface footing on cohesionless soil.

Over the last six decades, several experimental [4, 17-23] and numerical [13,24-31] studies have been conducted to predict S_γ values for rectangular footing with different aspect ratios (L/B), defined as the ratio of the footing's length (L) to its width (B). The S_γ equations recommended by researchers are outlined in Table 2. Terzaghi [1] recommended a constant S_γ value of 0.8 exclusively for square footings, based on the plate load test results reported by Golder [32]. Meyerhof [4], Hansen [17, 18], De Beer [19] and Perau [20] proposed semi-empirical S_γ equations derived from small-scale laboratory test results. Researchers [17-20] noted that S_γ values increase with an increase in aspect ratio (L/B) of footing, whereas Meyerhof [4] proposed the opposite trend. Furthermore, Meyerhof [4] and Hansen [18] stated that the internal friction angle of the soil influences S_γ values, while Refs. [17, 19, 20] argued that it has no impact.

Many of researchers have investigated the S_γ values using three-dimensional (3D) numerical models and laboratory model tests due to the large discrepancies in the semi-empirical recommendations. Michalowski [24] conducted numerical analyses based on upper bound limit analysis, utilizing a multi-block rupture mechanism. Michalowski [24] reported an increase in the S_γ value by increasing L/B for an internal friction angle less than 16°, while the maximum S_γ values were observed in square footing for higher internal friction angle values. Zhu and Michalowski [25] investigated the effect of aspect ratio of the footing on the S_γ values using a displacement-based finite element (*FE*) method. Researchers found that S_γ value initially increases with the L/B ratio, typically reaching a local peak, and then decreases as the L/B ratio continues to increase, particularly for cases where the internal friction angle exceeds 30°. Similar findings have been observed by several researchers [13, 26, 27, 30] using upper and lower bound based *FE* limit analysis, kinematic *FE* limit analysis and finite difference (*FD*) analysis. These researchers also noted that relationship between S_γ and L/B is influenced by the dilative characteristics of the soil and observed failure surface geometry of the footing. Lyamin et al. [13] performed 3D-*FE* upper and lower bound limit analysis to determine ultimate bearing capacity of a rectangular footing on sandy soil and reported that the differences between upper and lower bound results were found to be significant. Thus, these researchers recommended using the average of the corresponding lower and upper bound solutions to predict the ultimate bearing capacity. Shafiqul Islam et al. [28] studied the S_γ values of circular, square and strip footings through both laboratory model tests and 3D-*FE* analysis. They observed that ultimate bearing capacities of square footings were approximately 1.21 times higher than that of circular footing and S_γ values for both circular and square footing exceeded 1 when the internal friction angle was greater than 30°. Mohapatra and Kumar [29] and Osman [31] stated that both the bearing capacity and shape factor values increased with the roughness of the footing, as determined through rigorous finite element analysis.

Numerous studies in the literature have investigated the unit weight component of the shape factor (S_γ) values for footings with varying aspect ratios; however, conflicting findings have resulted in significant uncertainty for geotechnical designers when determining S_γ values for rectangular footings under field conditions. Therefore, in this study, rigorous parametric three-dimensional (3D) finite element (*FE*) analyses were conducted on sandy soil with the Hardening Soil (*HS*) model in PLAXIS 3D software to provide data on the S_γ values. In the

FE analyses, rectangular footings with seven different aspect ratios (*L/B*=1, 1.25, 1.5, 2, 3, 5, 10) and strip footing, along with sandy soil at four relative densities (D_r= 10%, 30%, 55%, 80%), were utilized to investigate the effects of footing geometry and internal friction angle on the N_γ and S_γ values. The N_γ and S_γ values obtained from 3D-*FE* analysis were compared with the recommendations in the literature to evaluate whether the existing methods are applicable to sandy soils. The failure mechanism of the footing with different aspect ratios at various relative densities was interpreted using the failure surface geometry obtained from the *FE* analysis results. Additionally, a new N_γ equation, based on the internal friction angle of the soil and a new S_γ equation, based on the internal friction angle of the soil and aspect ratio of the footing, were proposed to assist geotechnical designers in accurately predicting the ultimate bearing capacity of footings.

Table 2 - Summary of the S_γ equations in the literature

Researchers	S_γ	Methods	Remarks
Terzaghi [1]	0.8	Semi-empirical	Independent of the internal friction angle of the soil and recommended only for square footings.
Hansen [17]	$1-0.3\frac{B}{L}$	Semi-empirical	Independent of the internal friction angle of the soil.
Hansen [18]	$1-\frac{1}{2}(0.2+tan^6\phi)\frac{B}{L}$	Semi-empirical	-
Meyerhof [4]	$1+0.1\frac{B}{L}tan^2\left(45+\frac{\phi}{2}\right)$	Semi-empirical	-
De Beer [19]	$1-0.4\frac{B}{L}$	Semi-empirical	Independent of the internal friction angle of the soil.
Perau [20]	$\frac{1}{1+B/L}$	Semi-empirical	Independent of the internal friction angle of the soil.
Zhu and Michalowski [25]	$1+(0.6tan^2\phi-0.25)\frac{B}{L}$ for $\phi\leq 30^\circ$ $1+(1.3tan^2\phi-0.5)\left(\frac{L}{B}\right)^{1.5}e^{-\frac{L}{B}}$ for $\phi>30^\circ$	*FE* analysis using by ABAQUS	-
Lyamin et al. [13]	$1+(0.0336\phi-1.0611)\frac{B}{L}$	Upper-lower bound based *FE* limit analysis	-
Puzakov et al. [26]	$1+(0.6tan^2\phi-0.25)\frac{B}{L}$ for $\phi\leq 30^\circ$ $1+(1.3tan^2\phi-0.5)\left(\frac{L}{B}\right)^{1.55}e^{-0.9\frac{L}{B}}$ for $\phi>30^\circ$	*FD* analysis using by FLAC	-
Shafiqul Islam et al. [28]	$1+(1.8\phi^2-0.29)$	*FE* analysis using by ABAQUS	Recommended only for square footings.

Note: The design codes outlined by Eurocode 7 [32] recommend the use of the S_γ equation proposed by Hansen [17], while FHWA [33], AASHTO [34], CFEM [35] and GEO [36] recommend the use of the S_γ equation proposed by De Beer [19].

2. NUMERICAL SIMULATION

In this study, the pressure-settlement behavior of footings with different aspect ratios on cohesionless soil of different relative densities was simulated using commercial 3D-*FE* software (PLAXIS 3D, Version 20) to determine the unit weight component of the bearing capacity N_γ and shape factor (S_γ) values.

The Hardening Soil (*HS*) constitutive model, an elasto-plastic hyperbolic soil model, was chosen for its ability to perfectly simulate the non-linear and stress-dependent behavior of cohesionless soil. In contrast to conventional elastic-perfectly plastic models—such as Mohr-Coulomb and Drucker-Prager— which assume constant Young's modulus and neglect strain-dependent behavior, the *HS* model offers a more realistic and robust representation of soil response under varying loading conditions [37–40]. However, this model does not account for the post-peak softening behavior typically exhibited by dense cohesionless soil and over consolidated clay. The *HS* model captures the increase in soil stiffness during unloading-reloading, in contrast to the initial virgin loading. Furthermore, the *HS* model exhibits superior performance over conventional Duncan-Chang hyperbolic model by incorporating advanced plasticity principles that enable the realistic simulation of complex soil behaviors. These include the dilatancy effect, characterized by volume changes during shear deformation, a tension cut-off that captures the transition of dilating soils to a critical state where further dilatancy ceases, and a yield cap that accounts for irreversible plastic volumetric and shear strains arising from soil yielding.

In the present study, the footings were modeled as linear elastic plate structural elements due to their ability to efficiently simulate bending behavior, load transfer, and soil-structure interaction without the need for complex volumetric modeling. Similarly, several researchers [38-46] have recommended using plate structural elements for footing modeling. Additionally, a strength reduction factor (R_{int}) of 1 was applied to represent a fully rough condition (Equations (3)), where the interface friction angle (δ) between the soil and the footing is equal to the internal friction angle of the soil (ϕ).

$$R_{int} = \frac{tan\delta}{tan\phi} \tag{3}$$

The geometry of finite element (*FE*) models used in the parametric studies is shown in Figure 1 for both rectangular and strip footing. In the present study, only one-quarter of the total problem was modeled due to symmetry. Additionally, several researchers [13, 24-30] have conducted numerical studies using one-quarter or one-half of the total model to reduce analysis time and to better observe the failure surface geometry beneath the footing, as opposed to using the whole model. The soil volume boundary dimensions were established in accordance with recommendations from previous numerical and experimental studies in the literature [14, 25-30, 39-48]. Therefore, any potential side effects caused by the failure surface interacting with the outer boundaries of the soil volume were effectively eliminated. In the present study, the soil volume boundary dimensions were selected as 5*B* in the footing width direction and *L/2* + 4.5*B* in the footing length direction (Figure 1a) for rectangular footing analyses. To accurately simulate plane strain conditions in 3D-*FE* analyses with strip footings, the boundary dimension in the footing length direction was not extended and the length of the strip footing was assumed to be equal to 10*B*. However, the boundary dimension was extended a distance of 4.5 times the footing width beyond the periphery of the strip

footing (Figure 1b). Furthermore, for all *FE* models, depth of the soil volume was taken as 5*B*.

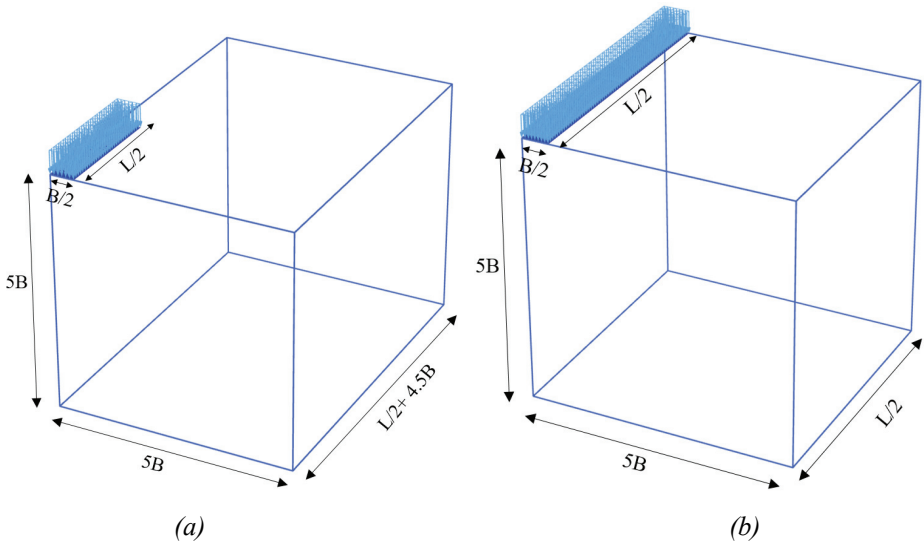

Figure 1 - Geometry of FE analysis: (a) rectangular footing; (b) strip footing

In the *FE* modeling, a fixed support condition was applied at the base of the soil volume to constrain movement in all three directions, thereby simulating the behavior of deeper soil layers that remain unaffected by the footing load and ensuring numerical stability. Simultaneously, simple support conditions were assigned to the side boundaries of the soil volume, preventing horizontal movement in both directions while allowing vertical displacement of the soil. This boundary configuration in the one-quarter model enables an accurate representation of the three-dimensional failure surface interaction, while avoiding unrealistic stress concentrations at the side boundaries. The boundary conditions adopted in this numerical study are consistent with those employed in previous research [13, 25–28, 31]. The effect of groundwater was not considered in these analyses. The soil cluster was discretized using 10-node tetrahedral volume elements, each with three translational degrees of freedom per node (u_x, u_y, u_z), while 6-node triangular plate elements were employed to simulate footing behavior. Additionally, 12-node elements were utilized for interfaces in the *FE* model to simulate the interaction between the soil and the footing or roughness of the footing. Furthermore, soil volume, plate and interface element consists of 4, 3 and 6 Gauss integration points, respectively, for evaluating stress-strain responses within each element. The simulation was carried out in two distinct phases. First, the initial stress field was established using the formula for the at-rest earth pressure coefficient as proposed by Jaky [48]. Then, an increasing uniform pressure was applied on the surface of the footings until collapse occurred in all *FE* analyses.

2.1. Verification of the Numerical Models

Verification of finite element (*FE*) analyses through experimental or in-situ testing is essential for ensuring the accuracy of numerical simulations [38, 42]. In this context, the laboratory model tests conducted by Khezri et al. [23], which involved footings with aspect ratios (*L/B*) of 1 and 2.25 placed on loose sand with a relative density of 35% and medium-dense sand with a relative density of 65%, were simulated in PLAXIS 3D using a quarter model. The pressure–settlement responses obtained from the physical experiments were subsequently compared with those derived from the numerical simulations. The laboratory model tests were carried out in a steel tank with internal dimensions of 800 mm × 1260 mm × 750 mm (width × length × height). A square footing measuring 150 × 150 mm and a rectangular footing measuring 100 × 250 mm were utilized, and the thickness of all footings was 20 mm. Furthermore, the internal friction angles of the loose and medium-dense Firouzkouh dry silica sands used in the experiments were reported as 35.2° and 37.7°, respectively. In the verification *FE* analyses, the dimensions of the test tank and footings, as well as the properties of the sandy soil and footings, were modeled to match those of the laboratory model test conditions. To enhance the accuracy of the simulations, a fine mesh density was employed. The footing pressure-settlement curves obtained from both the laboratory model tests and the *FE* analyses are presented in Figure 2. The results indicate that the outputs of the 3D-*FE* simulations were in good agreement with the experimental findings.

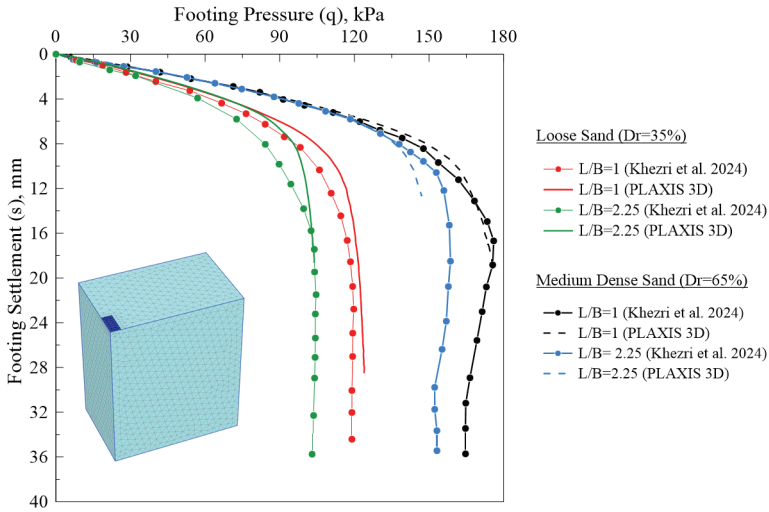

Figure 2 - Comparison of the laboratory model test with the numerical model

2.2. Parametric Studies

2.2.1. Properties of the Materials

The soil parameters utilized were derived from empirical equations proposed by Al-Defae et al. [49] for cohesionless sandy soil, as summarized in Table 3. In the present study, four distinct relative density values (D_r= 10, 30, 55 and 80%) were selected to investigate the effect of internal friction angle of soil, ranging from 31° to 45°, on the unit weight component

of the shape factors (S_γ). A relative density of 10% was incorporated into in the 3D-*FE* analysis to enrich the dataset for N_γ and S_γ values, despite the fact that sandy soils with a relative density below 25% are seldom encountered in field conditions.

Table 3 - The empirical HS parameter equations proposed by Al-Defae et al. [49]

Parameters	*Symbols*	Units	Equations
Dry unit weight	γ_{dry}	kN/m^3	14.5+3D_r/100
Saturated unit weight	γ_{sat}	kN/m^3	18.8+1.8D_r/100
Reference secant modulus	E_{50}^{ref}	kPa	1.25E_{oed}^{ref}
Reference tangent primary oedometer modulus	E_{oed}^{ref}	kPa	200D_r/100+2022
Reference unloading-reloading modulus	E_{ur}^{ref}	kPa	3E_{oed}^{ref}
Reference confining pressure	p_{ref}	kPa	100
Peak internal friction angle	ϕ	°	29+20D_r/100
Dilatancy angle	ψ	°	-4+25D_r/100≥0
Poisson's ratio for unloading-reloading	υ_{ur}	-	0.2
Exponential power	m	-	0.6-0.1D_r/100
Failure ratio	R_f	-	0.9

Table 4 - Implemented properties of the sandy soils with different relative density

Parameters	Unit	Values and Properties			
		***D*$_r$=10%**	***D*$_r$=30%**	***D*$_r$=55%**	***D*$_r$=80%**
-	-	*HS*	*HS*	*HS*	*HS*
-	-	Drained	Drained	Drained	Drained
γ_{dry}	kN/m^3	14.80	15.40	16.15	16.90
γ_{sat}	kN/m^3	18.98	19.34	19.79	20.24
E_{50}^{ref}	kPa	28400	34650	42462.5	50275
E_{oed}^{ref}	kPa	22720	27720	33970	40220
E_{ur}^{ref}	kPa	68160	83160	101910	120660
p_{ref}	kPa	100	100	100	100
ϕ	°	31	35	40	45
ψ	°	0	3.5	9.75	16
υ_{ur}	-	0.2	0.2	0.2	0.2
m	-	0.59	0.57	0.55	0.52
R_f	-	0.9	0.9	0.9	0.9

The use of small-scale model footings under laboratory conditions produced higher N_γ values than those predicted by theoretical recommendations or large-scale test results [6, 19, 40, 46]. This phenomenon, known as the scale effect, was attributed to lower confining stress levels. Moreover, Cerato and Lutenegger [46] observed in their experimental study that the discrepancy between N_γ values for circular and square footings on soil with three different relative densities (D_r=13%, 43% and 70%) was negligible for footing widths or diameters higher than 0.5 m. Thus, in this study, to eliminate the scale effect on the N_γ and S_γ values, the width of the footings was set at 1 m. The conventional parameters for C30 concrete, including unit weight, Young's modulus, and Poisson's ratio, were used for the footings. The properties of sandy soil with varying relative densities and footings are presented in Table 4 and Table 5, respectively.

Table 5 - Properties of the footings

Parameters	Symbols	Unit	Values and properties
-	-	-	Linear elastic
Young's modulus	E	kPa	32000
Shear modulus	G	kPa	13333.33
Unit weight	γ	kN/m^3	23.5
Poisson's ratio	υ	-	0.2
Thickness	d	m	0.1

2.2.2. Determining the Ultimate Bearing Capacity from Pressure-Settlement Curves

The footing pressure-settlement curves are used to determine ultimate bearing capacity from experimental and numerical analyses. Demirdöğen et al. [47] discussed five distinct approaches for estimating the ultimate bearing capacity derived from the pressure-settlement curve, namely the tangent intersection method, the 0.1B method, the minimum slope method, the log-log method, and the semi-log method. These methods yield varying ultimate bearing capacity values, and the minimum slope and log-log methods are not applicable to loose or very loose sandy soils [47, 50]. In the present study, the tangent intersection method was selected due to its widespread use in interpreting the ultimate bearing capacity of footings, particularly in PLAXIS 3D analyses [41-44, 51-53] as illustrated in Figure. 3.

2.2.3. Program of the Parametric Finite Element Analyses

In the present study, three series of parametric finite element (*FE*) analyses were performed. In all *FE* analyses, the footing width was assumed to be constant at 1 m. Series A was conducted to determine the appropriate mesh density for use in the other *FE* analysis series, with the *L/B* ratio and D_r were kept constant. Series B focused on estimating N_γ values for strip footings, while Series C aimed to determine S_γ values for rectangular footings with varying aspect ratios (*L/B*), ranging from 1 to 10. Additionally, to investigate the effect of relative density or internal friction angle on the N_γ and S_γ values, analyses were carried out for 4 different relative densities, ranging from 10% to 80% in both Series B and C. The program of the parametric *FE* analyses is presented in Table 6.

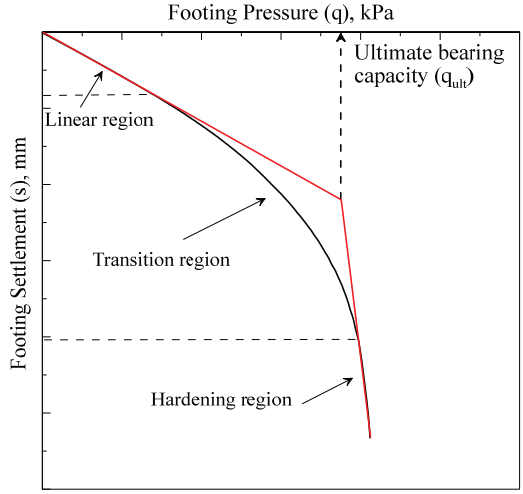

Figure 3 - Determination ultimate bearing capacity of the footing from pressure-settlement curve using tangent intersection method

Table 6 - Implemented properties of the sandy soils with different relative density

Series	Footing type	Variable parameters	Constant parameters	Purpose of analyses
A	Rectangular	Mesh density: very coarse, coarse, medium, fine, very fine	B=1 m L/B=1.5 D_r=55%	The effect of mesh density
B	Strip	D_r=10%, 30%, 55%, 80%	Fine mesh B=1 m L/B=10	The effect of relative density on the N_γ values
C	Rectangular	L/B=1, 1.25, 1.5, 2, 3, 5, 10 D_r=10%, 30%, 55%, 80%	Fine mesh B=1 m	The effect of aspect ratio and relative density on the S_γ values

3. RESULTS AND DISCUSSIONS

3.1. Mesh Density

PLAXIS 3D *FE* software provides five distinct mesh densities, ranging from very coarse to very fine. As it well known, mesh density affects the accuracy of the finite element model and the computing time. Therefore, mesh sensitivity analyses were conducted in Series A (Figure 4). The result of Series A revealed that the difference between in the ultimate bearing capacity (q_{ult}) values obtained from fine mesh compared to very fine mesh was less than 0.4%. However, the very coarse, coarse and medium meshes led to an overestimation of the ultimate bearing capacity compared to the fine and very fine mesh densities. Consequently, a fine mesh density was selected for Series B and C to achieve a balance between high accuracy and computational efficiency.

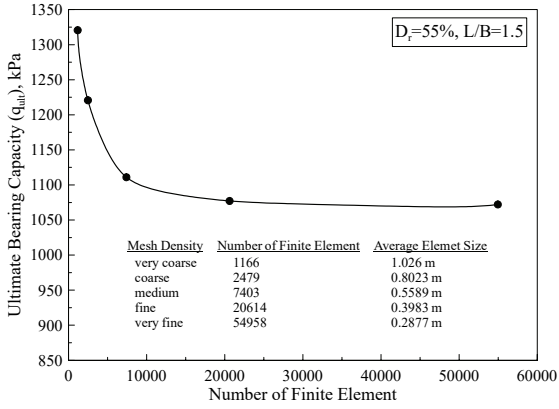

Figure 4 - The effect of mesh density on the ultimate bearing capacity

3.2. Unit Weight Component of the Bearing Capacity Factor Values

The variation of the effective unit weight component of the bearing capacity factor (N_γ) values, derived from PLAXIS 3D finite element analyses conducted with various relative densities (D_r) or internal friction angles (ϕ) on sandy soil for strip footings are illustrated in

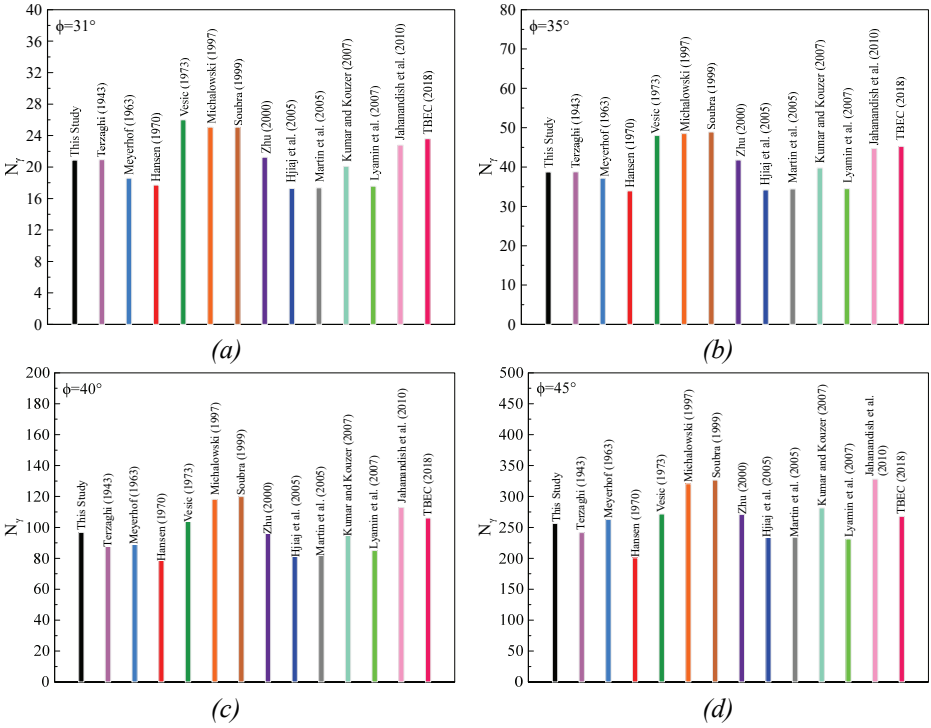

Figure 5 - Comparison of the N_γ values obtained from PLAXIS 3D and theoretical recommendations: (a) ϕ=31°; (b) ϕ=35°; (c) ϕ=40°; (d) ϕ=45°.

Figure 5. In this study, N_γ values were obtained as 20.9, 38.7, 96.7, and 256.5 for sandy soil with internal friction angles of 31°, 35°, 40° and 45°, respectively and were compared with theoretical recommendations from the literature [1, 4-16]. It was observed that the N_γ values obtained from PLAXIS 3D were consistent with those in the literature, particularly the recommendations of Refs. [9, 12, 16]. Consequently, it was concluded that the footing width used in the *FE* analyses was sufficiently large to eliminate scale effects, and that PLAXIS 3D provided highly accurate predictions of ultimate bearing capacity of shallow footings.

3.3. Unit Weight Component of the Shape Factor Values

The footing pressure-settlement curves obtained from 3D-*FE* analyses in both Series B and C for rectangular footings with different aspect ratios (*L/B*) and strip footing under different relative densities are presented in Figure 6. The results of the *FE* analyses revealed that an

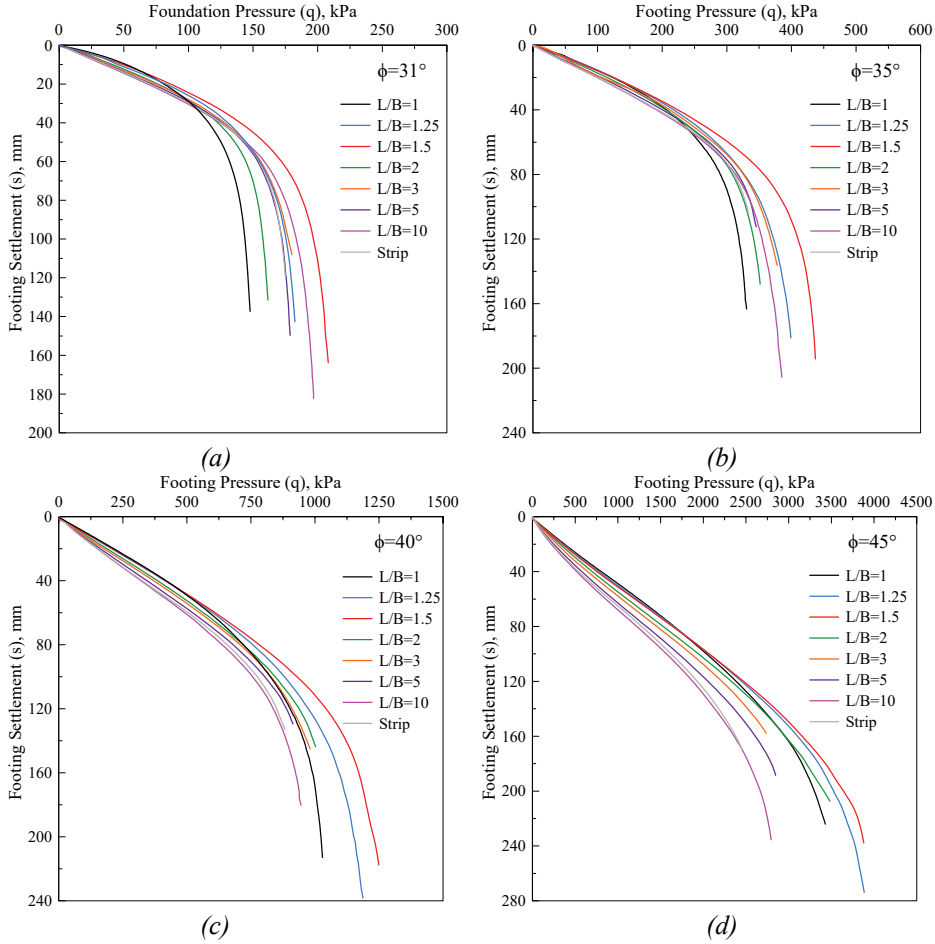

Figure 6 - The obtained pressure-settlement curves from FE analyses in Series B and C for: (a) ϕ=31°; (b) ϕ=35°; (c) ϕ=40°; (d) ϕ=45°

increase in relative density or internal friction angle increased both the initial stiffness of the pressure-settlement curves and the bearing pressure performance. It was observed that as the relative density increased, the linear region of the pressure-settlement curve extended, while the transition and hardening regions contracted. Furthermore, *L/B* ratio of the footing is also a key parameter influencing the ultimate bearing capacity (q_{ult}), as demonstrated in Figure 6.

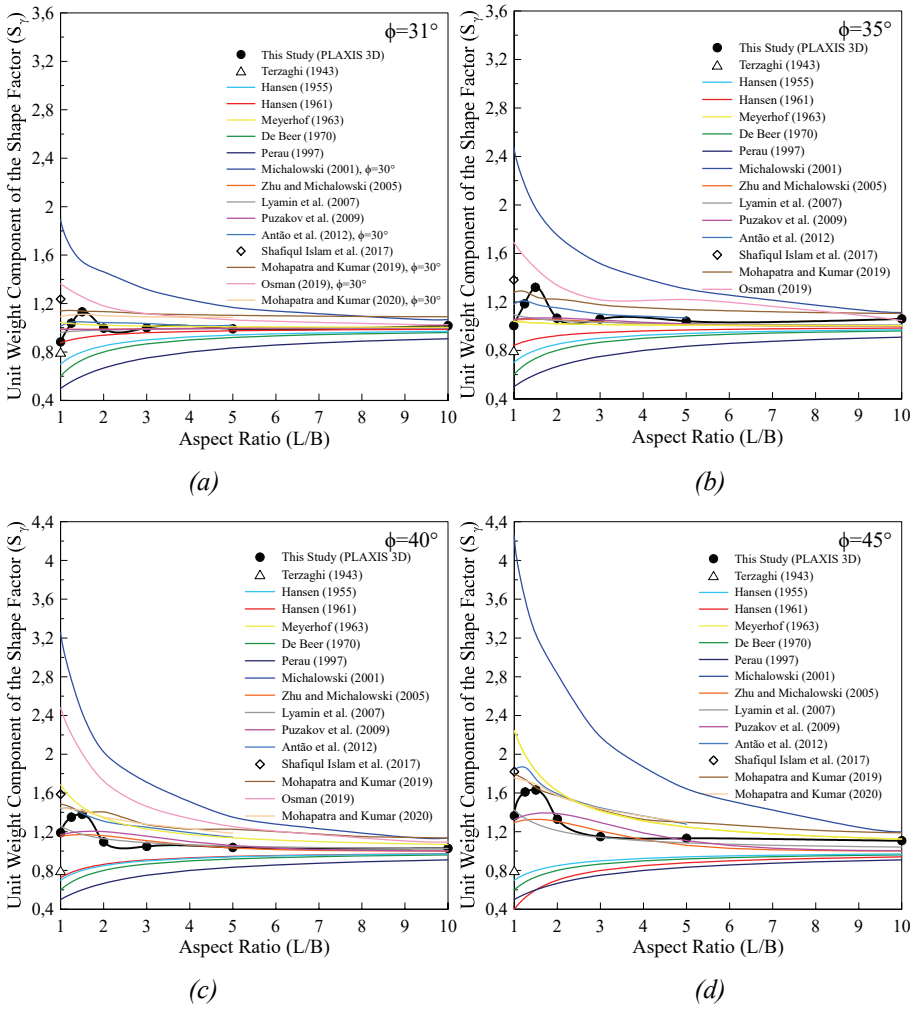

Figure 7 - The comparison of the S_γ values obtained from PLAXIS 3D with the recommendations of various researchers for: (a) ϕ=31°; (b) ϕ=35°; (c) ϕ=40°; (d) ϕ=45°

The S_γ values obtained from 3D-*FE* analyses for rectangular footings with different *L/B* ratios (*L/B*=1, 1.25, 1.5, 2, 3, 5, 10) on sandy soil with different relative densities (D_r=10%, 30%, 55%, 80%) are presented in Figure 7. Moreover, obtained S_γ values are compared with the recommendation provided by various researchers [1, 4, 13, 17-20, 24-31]. It was observed

that the S_γ values obtained from this 3D-*FE* study varied between 0.88 and 1.63 depending on relative density (D_r) of the soil and aspect ratio (L/B) of the footing generally aligning with the numerical results reported in Refs. [25-27, 29, 30].

In this study, it was observed that S_γ values initially increased as the L/B ratio increased, reaching a maximum value at L/B=1.5 across all relative densities of sandy soil. Beyond this point, the values declined as after the L/B ratio continued to increase, although the rate of decrease diminished significantly for $L/B \geq 3$. Similarly, several researchers [13, 25-27, 29, 30] reported that local peak S_γ values occurring between L/B=1 and L/B=2.5. However, the findings of this study contradict conventional semi-empirical approaches [1, 17-20], which propose that the maximum S_γ value occurs for strip footings and the minimum S_γ value is observed for square footings. Additionally, it should be noted that current design codes [32-36] and geotechnical reference books [50, 54-59] continue to recommend the use of the unit weight component from the shape factor (S_γ) equation proposed by Hansen [17] and De Beer [19] for shallow footings. Furthermore, the S_γ values exhibited a tendency to increase with increasing internal friction angle or relative density of the soil beneath the footing, as shown in Figure 6, aligning well with current numerical approaches [13, 23-30] and the recommendations of Meyerhof [4]. This finding contrasts with the semi-empirical recommendation of Terzaghi [1], Hansen [17], De Beer [19] and Perau [20] stated that S_γ values are independent of the internal friction angle of the soil. It also contradicts Hansen [18], who reported that S_γ values decrease as the internal friction angle increases. The discrepancies between the S_γ values observed in this study and those reported in previous numerical studies can be attributed to several factors: variations in the methods used for determining ultimate bearing capacity, in the numerical analysis techniques (upper and lower bound limit analysis, finite element analysis, finite difference analysis), and in the details of the numerical models, including the constitutive soil model, soil modulus, dilatancy angle, Poisson's ratio, mesh size, finite element type.

3.4. Failure Mechanism

The relationship between S_γ values and L/B ratio of the footing, along with the internal friction angle of the sandy soil beneath the footing exhibits significant complexity. This complex behavior can be attributed to the influence of failure surface, which is defined as the region where incremental deviatoric strains are localized or as the boundary of the incremental displacement field. Therefore, in this study, incremental deviatoric strains and incremental displacements obtained from PLAXIS 3D *FE* software were investigated to interpret the failure mechanism of footings with different aspect ratios on sandy soils with different relative densities. The contours of incremental deviatoric strains and incremental displacements for rectangular footings with aspect ratios of 1.5 and 3 and, as well as strip footings on sandy soil at the time of failure from 3D-*FE* analyses with two different internal friction angles of 31° and 45° are presented in Figure 8 and Figure 9, respectively. As can be seen in Figure 8 and Figure 9, in the zone outside the failure surface, the value of incremental deviatoric strains and incremental displacements were almost zero due to the absence of soil shear deformation that would cause plasticity. An inverted pyramidal wedge forms beneath the footing, moving vertically downward like a rigid body. The failure surface exhibits a curvilinear shape beneath the footing, transitioning to a planar form near the soil surface. Furthermore, the failure surface geometry on the quarter soil model, except for strip footing,

viewed from above, consisted of two distinct half-elliptical shapes extending from the edges of the footings. In contrast the geometric shape for strip footings is similar to rectangular.

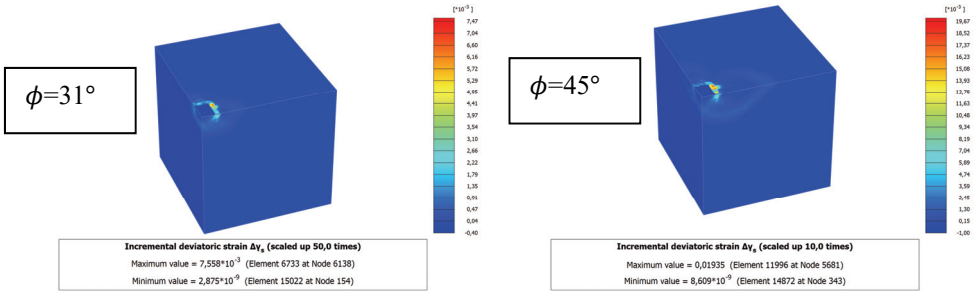

(a)

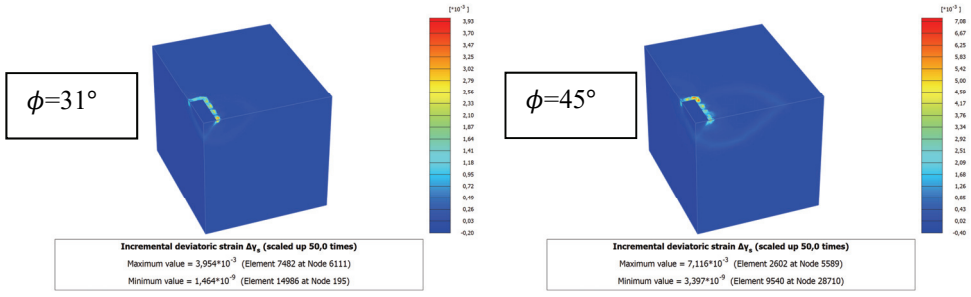

(b)

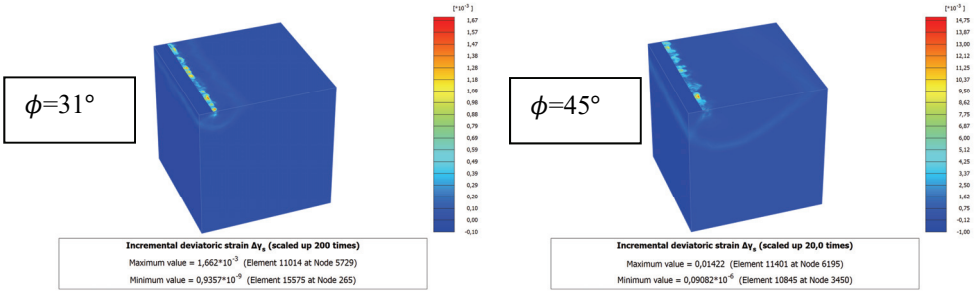

(c)

Figure 8 - The variation of the incremental deviatoric strains on soil with internal friction angle of 31° and 45° for: (a) L/B=1.5; (b) L/B=3 (c) strip footing

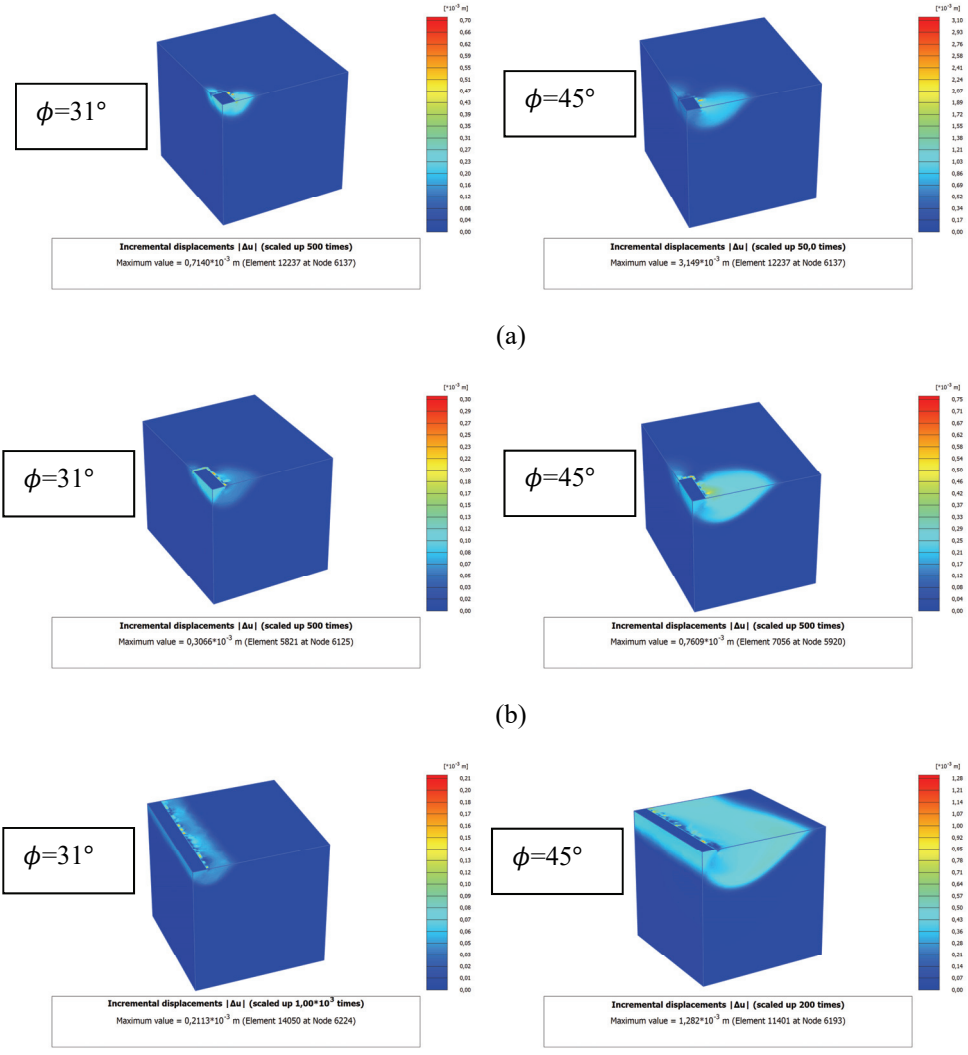

Figure 9 - The variation of the incremental displacement on soil with internal friction angle of 31° and 45° for: (a) L/B=1.5; (b) L/B=3 (c) strip footing

The results of the *FE* analyses showed that the boundary of the failure surface, along with the maximum incremental deviatoric strain and incremental displacement values, increased with increasing relative density of the cohesionless soil. This is attributed to increase in the internal friction and dilation angles, consistent with the findings reported in Refs. [25-27, 29-31]. As the internal friction angle increases, the shear strength of the soil improves, while a higher dilation angle requires more energy for shearing, causing the soil to resist deformation

across a wider region. Moreover, it was observed that the intensity of localized incremental deviatoric strains increased in the radial wedge and passive zone of the failure surface as the relative density of the soil increased. Similarly, incremental displacement contours were concentrated underneath the footing or the active zone of the failure surface under the D_r = 10% condition, forming a nearly smooth arc-shaped geometry. However, as the relative density of the sandy soil increased, the displacement contours transitioned to a more extended and inclined geometry and became distributed across all zones of the failure surface, including the active zone, radial wedge, and passive zone. As a result, unit weight component of the shape factor (S_γ) values increased with increasing relative density of cohesionless soil due to changes in the failure surface geometry, enlargement of the failure surface, and intensification of three-dimensional interactions within the failure surface [25, 31].

The maximum incremental deviatoric strains and incremental displacements were observed around the rectangular footings, whereas for strip footings, these maximum values were concentrated along the length of footing due to the constraint of the failure surface in the direction of footing's length, simulating a plane strain condition, illustrated in Figures 8 and 9. This observation aligns with the findings of Janabi et al. [22] and Mohapatra and Kumar [29, 30]. Moreover, failure surface boundary for square footings were almost identical both in length and width direction of the footing. However, as the *L/B* ratio increased, the three-dimensional failure surface boundary contracted along the footing length and expanded along the footing width. Consequently, the failure surface boundary reached its maximum in the direction of the footing width and its minimum in the direction of the footing length, particularly for strip footings. Similar results have been reported by several researchers [25-27, 29-31]. Thus, it is believed that the three-dimensional geometry and the interaction of the failure surface influence the magnitude of passive forces within the failure surface, which in turn affects the ultimate bearing capacity. These factors lead to the highest values of q_{ult} and S_γ, along with incremental deviatoric strains and incremental displacements, occurring at an *L/B* ratio of 1.5 across all relative density levels, when compared to other rectangular and strip footings (Figures 7-9). In addition to these factors, Zhu and Michalowski [25] and Puzakov et al. [26] reported that this phenomenon is closely related to the ratio of the volume of displaced soil or failure surface to the area of the footing, denoted as r_v, because a larger volume of the failure surface contributes to increasing shear resistance. Their findings indicated that this ratio reaches its maximum for strip footings and decreases as the *L/B* ratio decreases, particularly when the internal friction angle of the soil is less than 30°. However, for soils with higher friction angles (ϕ>30°), the dilative behavior of the soil has a more pronounced effect on increasing the volume of displaced soil beneath rectangular footings within the *L/B* ratio range of 1 to 2.5 than other rectangular and strip footings. Although the r_v values could not be directly calculated in the present study, qualitative comparisons—based on the observed soil volumes affected by incremental displacements and the intensity of concentrated incremental deviatoric strains in the soil profile—suggest that the maximum r_v value occurs at *L/B* = 1.5 (Figures 8 and 9).

3.5. Unit Weight Component of the Shape Factor Equation Proposal

Non-linear multiple regression analysis with upper and lower confidence limit 95% was performed using SPSS V27 statistical software to derive a mathematical equation for N_γ for strip footings and S_γ values of rectangular footings on sandy soil, based on results from

PLAXIS 3D *FE* analyses. In this regression analysis, a total 120 data points, including both input and output variables, were utilized. The internal friction angles (ϕ) of the sandy soil and the aspect ratios (L/B) of the rectangular footing were taken as input dependent parameters to estimate S_γ values, whereas only the internal friction angles of soil were used as input dependent parameter for predicting N_γ values. The result of the non-linear multiple regression analyses for determining N_γ and S_γ are given in Equations (4) and (5), respectively. The coefficient of determination (R^2), mean absolute error (*MAE*), root mean square error (*RMSE*) values were found to be 0.98, 0.65 and 0.68 for Equation (4) and, 0.92, 0.05 and 0.05 for Equation (5), respectively.

$$N_\gamma = e^{0.52+5.02tan\phi}\tan(\phi) \tag{4}$$

$$S_\gamma = 0.74 + 0.34tan\phi + (-1.53 + 8.88tan\phi^2)e^{-12.09\frac{L}{B}-0.02tan\phi+8.66}L/B^{\,17.12} \tag{5}$$

A two-sample t-test was employed to evaluate the significance of the differences between the proposed N_γ and S_γ equations those recommended in the literature. Accordingly, the corresponding P-values—statistical metrics that indicate whether the observed differences could have occurred due to random chance—were computed (Table 7). A significance level (α) of 0.05, commonly used in statistical analysis, was adopted; P-values less than this threshold indicate statistically significant differences [74, 75]. As shown in Table 7, P-values for all N_γ recommendations exceed 0.05, whereas among the S_γ recommendations, only those from Refs. [13, 25, 26] and the output of the 3D numerical analyses exceed this threshold. These findings indicate that the predicted N_γ values from Equation (4) do not show statistically significant differences from those in references [1, 4–14]. Furthermore, the predicted S_γ values from Equation (5) do not differ significantly from those proposed by Lyamin et al. [13], Zhu and Michalowski [25], and Puzakov et al. [26], as well as from the present finite element (*FE*) study. Therefore, these recommendations are reliable and suitable for the prediction of N_γ and S_γ values.

To assess the accuracy of the proposed equations, the $N_\gamma \times S_\gamma$ results from 56 in-situ plate tests, laboratory plate tests, and centrifuge tests on cohesionless soils reported in the existing literature, as presented in Table 8, were compared with the values predicted by Equations (4) and (5) in Figure 10. In Table 8, data involving rectangular and strip surface footings with widths greater than 0.15 m were collected from the literature, as the N_γ and S_γ values obtained from smaller footings may be influenced by scale effects, despite the existence of numerous small-scale laboratory model tests in the geotechnical literature. As shown in Figure 10, the proposed equations demonstrate high accuracy and minimal bias in estimating $N_\gamma \times S_\gamma$ values for rectangular and strip footings on cohesionless soils, with predictions consistently aligning with actual measurements (R^2=0.91, *RMSE*=33.4, *MAE*=22.6). Consequently, instead of relying on traditional semi-empirical equations—which often neglect the effect of internal friction angle and assume that the maximum S_γ value corresponds to strip footings, as commonly suggested by design codes and geotechnical references-engineers can adopt the proposed equations to achieve more accurate predictions of the ultimate bearing capacity of footings on cohesionless soils and resulting in more reliable and cost-efficient footing designs.

Table 7 - Results of statistical analyses

N_γ				S_γ			
Researchers	**P value**	**Researchers**	**P-value**	**Researchers**	**P value**	**Researchers**	**P-value**
Terzaghi [1]	0.954	Martin et al. [11]	0.897	Meyerhof [4]	0.044	Lyamin et al. [13]	0.602
Meyerhof [4]	0.995	Kumar and Kouzer [12]	0.926	Hansen [17]	2.080×10^{-9}	Puzakov et al. [26]	0.676
Hansen [5]	0.781	Lyamin et al. [13]	0.888	Hansen [18]	7.831×10^{-8}	Antão et al. [27]	0.016
Vesic [6]	0.888	Jahanandish et al. [14]	0.788	De Beer [19]	1.418×10^{-10}	Mohapatra and Kumar [29]	1.838×10^{-3}
Michalowski [7]	0.775	Kumar and Khatri [15]	0.778	Perau [20]	7.904×10^{-14}	Mohapatra and Kumar [30]	3.520×10^{-3}
Soubra [8]	0.761	TBEC [16]	0.920	Michalowski [24]	1.528×10^{-6}	Osman [31]	0.013
Zhu [9]	0.936	This Numerical Study	0.993	Zhu and Michalowski [25]	0.344	This Numerical Study	0.590
Hjiaj et al. [10]	0.898						

Table 8 - A database of footing on cohesionless soil used for validation of recommended equations

Reference	Description	B (m)	L (m)	L/B	γ' (kN/m^3)	ϕ (°)	$N_\gamma \times S_\gamma$
Meigh and Nixon [60]	In-situ plate load test	0.31, 0.75	0.31, 0.75	1	16.2	40.2	103.5-186.5
Rodin [61]	In-situ plate load test	0.3	0.3	1	20.8	41.4-47.5	135.3-541.3
Thornburn [62]	In-situ plate load test	0.31	0.31	1	15.8	36.8	98.5
Aliban and Znidarčić [63]	Centrifuge tests	1.14 for 15g	3.42 for 15g	Strip	17.2	44	219.6, 229.2
Adams and Collins [64]	Large-scale laboratory model test	0.46-0.91	0.46-0.91	1	14.2-14.7	28-35.9	21.7-71.9
Mestat and Berthelon [65]	In-situ plate test	0.7, 1	0.7, 1	1	16.8	39.6	59.5-126.9
Siddiquee et al. [66]	Laboratory model test	0.23	0.23-0.45	1-1.95	15.5-16	41-42	143.2-180.5
Cerato and Lutenegge [46]	Laboratory model test	0.305-0.914	0.305-0.914	1	7.4, 9.6	34.3, 35.6	42-82
Mosallanezhad et al. [67]	Laboratory model test	0.2	0.2	1	18.7	43	188.5
Ziccarelli et al. [68]	Centrifuge tests	1 for 25g 1.6 for 40g	4 for 25g 6.4 for 40 g	Strip	15.8	47	377.1-489.7
Kyparissis and Lopes [69]	Centrifuge tests	0.75 for 30g	2.85 for 30 g	Strip	16.3	31.7	26.4
Shadman et al. [70]	Large-scale laboratory model test	0.25-0.6	0.25-0.6	1	16.1-17.2	38, 41	65.6-154
Wang et al. [71]	Laboratory model test	0.5	0.5	1	18.1	39	137.1
Bharti et al. [72]	Laboratory model test	0.18	0.24	1.33	16	40.1	121.5
Gupta and Mital [46]	Laboratory model test	0.18	0.34	1.33	17.5	36	92.1
Latha et al. [73]	Laboratory model test	0.2	0.2	1	17.5	35	41.4

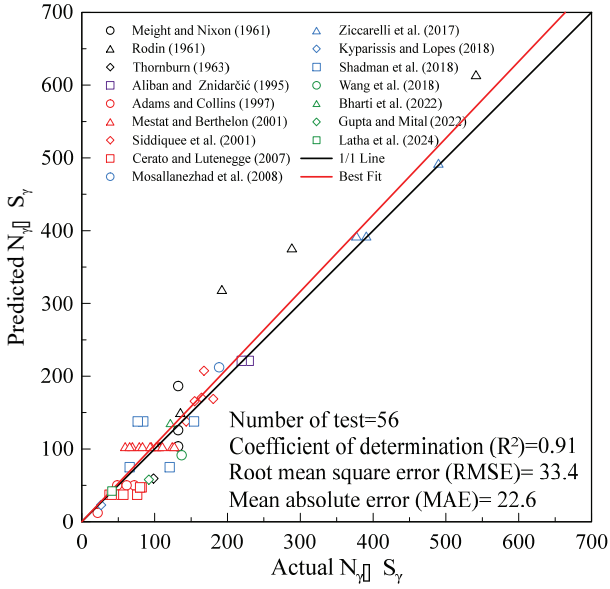

Figure 10 - Comparison of the $N_\gamma \times S_\gamma$ values predicted by the recommended equations and actual measurements

3.6. Limitations of This Numerical Study

The limitations of this three-dimensional (3D) numerical study regarding the influence of the footing's aspect ratio (L/B) on the unit weight component of bearing capacity (N_γ) and the shape factor (S_γ) for footings on sandy soils with varying relative densities are summarized as follows:

- This 3D finite element study focuses on surface rectangular and strip footings placed on homogeneous sandy soil, using soil parameters derived from empirical equation proposed by Al-Defae et al. [47] for four different relative densities (D_r= 10, 30, 55, 80%).
- The footings are subjected to axial loading.
- Footing width was selected as 1 m to eliminate scale effect. Small-scale test results may yield different N_γ and S_γ values due to influence of lower confining stress.
- Seven distinct aspect ratios (L/B= 1, 1.25, 1.5, 2, 3, 5, 10) of the rectangular footings were utilized.
- One-quarter of the whole model was analyzed in this study due to geometric symmetry and in order to reduce analysis time. However, minor discrepancies may exist between the results obtained from this ¼ of the whole model and those that would be derived from a whole model.

- The soil volume boundary dimensions were chosen to be sufficiently large to mitigate side effects, with fixed supports applied at the base of the model and simple supports at the sides as boundary conditions. However, additional analyses are necessary for alternative scenarios (e.g., interfering footings, sloped ground conditions) where the problem geometry and boundary conditions differ, as these variations could influence stress and displacement distributions, as well as the three-dimensional geometry of the failure surface.
- The footing is modeled as fully rough condition. It is important to note that footing roughness effects the geometry and border of failure surface, and consequently, affect the ultimate bearing capacity [7, 10, 13, 24, 29-31, 76, 77] and failure surface geometry.
- The influence of the presence of groundwater on the N_γ and S_γ values was not investigated in this study. Several researchers [76–78] have reported that the position of the groundwater table significantly affects the bearing capacity of footings by reducing the effective weight of the soil, particularly under drained conditions. Moreover, Cascone et al. [60] observed that the location of the water table also alters the extent and intensity of the plastic strain volume zone that develop beneath the footing.
- The Hardening Soil (*HS*) model was selected as the constitutive soil model because it effectively simulates the non-linear, stress-dependent hardening behavior of the cohesionless soils and demonstrates superior performance in predicting footing pressure-settlement responses up to the peak failure pressure. However, it does not account for the post-peak strain softening behavior of dense sands or overconsolidated clays, which is characterized by a progressive reduction in shear strength with continued deformation beyond the peak stress. Consequently, the *HS* model tends to underestimate deformations in scenarios where strain softening plays a significant role—particularly under cyclic or seismic loading, time-dependent (creep) loading, and load levels approaching or exceeding the footing's ultimate bearing capacity.

4. CONCLUSIONS

In this study, a rigorous parametric numerical analyses were conducted into the unit weight component of the shape factors (S_γ), footing pressure-settlement responses and ultimate bearing capacities (q_{ult}) for rectangular footings on sandy soil, employing three-dimensional finite element (*FE*) analyses using PLAXIS 3D software. The analyses investigated the influence of footing geometry and relative density of sandy soil on the S_γ values and failure mechanism, encompassing a broad spectrum of aspect ratios (L/B=1 to 10) and internal friction angles (31° to 45°). The key conclusions drawn from the results presented in this paper are as follows:

- The unit weight component of the bearing capacity factor (N_γ) values obtained from PLAXIS 3D using the Hardening Soil (*HS*) constitutive model are consistent with the recommended equations derived empirically, analytically and numerically in the literature.

- The *L/B* ratio was found to be a critical parameter affecting the ultimate bearing capacity, the S_γ value and the behavior of the footing pressure-settlement response. The findings revealed that the S_γ values initially increased with the *L/B* ratio, peaking at *L/B*=1.5 and then gradually decreased as the *L/B* ratio continued to rise due to three-dimensional interaction of the failure surface, failure surface geometry and volume of displaced soil particles. However, the rate of reduction diminished significantly when the *L/B* ratio exceeded 3. The results of this study indicate that the traditional semi-empirical methods recommended by numerous researchers [17-20], which propose that the highest S_γ values occur in strip footings, are insufficient for accurately representing S_γ values for footings on sandy soil. However, for cases where the *L/B* ratio was greater than or equal to 5, a discrepancy of 5% to 21% was observed in the S_γ values between the *FE* analysis results obtained in this study and the recommendations outlined in Hansen [17, 18], De Beer [19] and Perau [20].

- The finite element analysis results indicated that internal friction angle or relative density of the sandy soil influences the behavior of the footing pressure-settlement curve, ultimate bearing capacity and S_γ value. It was observed that S_γ values increased with increasing internal friction angle, which contradicts the pre-existing methods [1, 17-20] but aligns with the findings of several researchers [4, 13, 24-31]. An increase in the internal friction angle of the sandy soil led to the expansion of the failure surface, with the radial wedge and passive zone becoming more pronounced. Moreover, the geometry of the failure surface transitioned from a nearly smooth arc shape to a more inclined curvilinear form.

- It was observed that traditional semi-empirical approaches [17-20] result in up to a 3.41-fold underestimation of the S_γ values compared to those obtained from the *FE* analyses in this study, whereas the findings of Michalowski [24] and Osman [31] lead to an overestimation of the S_γ values by up to 3.12 times. Furthermore, the S_γ values obtained from this 3D-*FE* study generally consistent with the findings of Refs. [25-27, 29, 30].

- Non-linear multiple regression analyses were performed using data obtained from three-dimensional finite element analyses, leading to the development of the N_γ equation for strip footings and the S_γ equation for rectangular footing with different aspect ratios. All proposed equations exhibited high coefficients of determination (R^2) alongside low mean absolute error (MAE) and root mean square error (RMSE) values,

- Conventional equations [17, 19] prescribed in current design codes [32-36] and geotechnical reference books often lack sufficient accuracy in predicting S_γ values, as such equations neither comprehensively represent the relationship between the S_γ and *L/B* nor incorporate the influence of the internal friction angle. This results in an underestimation of the ultimate bearing capacity of rectangular footings on cohesionless soils, potentially resulting in overly conservative designs and increased construction costs. Accordingly, it is recommended that existing design codes and reference materials be updated in line with the findings of this study and recent research in the literature.

The results of this study highlight the influence of the aspect ratio of footings, as well as the relative density of the sandy soil, on the unit weight component of the bearing capacity and shape factor values. However, this study has certain limitations and there are numerous

research avenues and shortcomings that require further investigation. In the future, fully instrumented large-scale, centrifuge, or in-situ tests should be conducted to investigate the influence of footing geometry on ultimate bearing capacity, pressure–settlement behavior, surface settlement profiles, and stress distribution patterns. Such studies will offer a more accurate and realistic representation of in-situ behavior, addressing the limitations and scale effects inherent in small-scale laboratory tests that dominate the current literature. Consequently, these efforts will contribute to a more reliable dataset and a deeper understanding of footing failure mechanisms. Moreover, there is a need to develop generalized dimensionless equation for the unit weight component of the shape factors, aimed at helping geotechnical engineers more accurately predict the ultimate bearing capacity. This equation should consider the influence of a broad range of soil parameters—including internal friction angles from 0° to 45°, dilatancy angles up to the peak internal friction angle, as well as variations in modulus of elasticity and Poisson's ratio—along with footing roughness and groundwater table position. The footing embedment depth factors, surcharge and cohesion component of the bearing capacity and shape factors should be updated through a combination of numerical modeling and experimental validation. Furthermore, the behavior of footings subjected to complex loading scenarios—including inclined, eccentric, cyclic, seismic, and long-term (creep) loading—should be systematically investigated to build a more comprehensive understanding of the performance of footings with various geometric configurations.

Data Availability Statement: All data, models, and code generated or used during the study appear in the submitted article. Some or all data, models, or code that support the findings of this study are available from the corresponding author upon reasonable request.

Conflicts of Interest: The authors declare no conflicts of interest.

Ethics Approval: There are no relevant waivers or approvals.

Consent to Participate: Not applicable.

Consent for Publication: The authors allows publication if the research is accepted.

Financial interests: The authors declare they have no financial interest

References

[1] Terzaghi, K., Theoretical Soil Mechanics, 1st ed., New York, USA. Wiley, 1943.

[2] Prandtl, L. Über Die Harte Plastischer Körper, Nachrichten Von Der Könighlichen Gesellschaftder Wissenschaften Zur Göttingen, Mathematisch-Physikalischen Klasse, 1, 15-20, 1920.

[3] Reissner, H., Zum Erddruckproblem, 1st International Congress for Applied Mechanics. Delft, The Netherlands, 1924.

[4] Meyerhof, G. G., Some Recent Research on the Bearing Capacity of Foundations. Canadian Geotechnical Journal, 1(1), 16-26, 1963.

[5] Hansen, J. B., A Revised and Extended Formula for Bearing Capacity. Danish Geotechnical Institute, 28, 5–11, 1970.

[6] Vesic, A. S., Analysis of Ultimate Loads of Shallow Foundations. Journal of the Soil Mechanics and Foundations Division, 99(1), 45-73, 1973.

[7] Michalowski, R., An Estimate of the Influence of Soil Weight on Bearing Capacity Using Limit Analysis. Soils and Foundations, 37(4), 57-64, 1997.

[8] Soubra, A. H., Upper-Bound Solutions for Bearing Capacity of Foundations. Journal of Geotechnical and Geoenvironmental Engineering, 125(1), 59-68, 1999.

[9] Zhu, D., The Least Upper-Bound Solutions for Bearing Capacity Factor Nγ. Soils and Foundations, 40(1), 123-129, 2000.

[10] Hjiaj, M., Lyamin, A.V., Sloan, S.W., Numerical Limit Analysis Solutions for the Bearing Capacity Factor Nγ. International Journal of Solids and Structures, 42(5-6), 1681-1704, 2005.

[11] Martin C. M., Exact Bearing Capacity Calculations Using the Method of Characteristics, 11th International Conference of the International Association for Computer Methods and Advances in Geomechanics, Turin, Italy, 2005.

[12] Kumar, J., Kouzer, K. M., Effect of Footing Roughness on Bearing Capacity Factor Nγ. Journal of Geotechnical and Geoenvironmental Engineering, 133(5), 502-511, 2007.

[13] Lyamin, A.V., Salgado, R., Sloan, S.W., Prezzi, M., Two-and Three-Dimensional Bearing Capacity of Footings in Sand. Géotechnique, 57(8), 647-662, 2007.

[14] Jahanandish, M., Veiskarami, M., Ghahramani, A., Effect of Stress Level on the Bearing Capacity Factor, Nγ, by the ZEL Method. KSCE Journal of Civil Engineering, 14, 709-723, 2010.

[15] Kumar, J., Khatri, V. N., Bearing Capacity Factors of Circular Foundations for a General C–Φ Soil Using Lower Bound Finite Elements Limit Analysis. International Journal for Numerical and Analytical Methods in Geomechanics, 35(3), 393-405, 2011.

[16] TBEC. Turkey Building Earthquake Code. Ministry of Environment and Urbanization of Türkiye. 2018.

[17] Hansen, J. B., Simpel Beregning af Fundamenters Bæreevne. Ingeniøren, 22(1) 95-100, 1955.

[18] Hansen, J. B., A General Formula for Bearing Capacity, Bulletin No. 11, Danish Geotechnical Institute, Copenhagen, Denmark, 1961.

[19] De Beer, E. E., Experimental Determination of the Shape Factors and the Bearing Capacity Factors of Sand. Géotechnique, 20(4), 387-411, 1970.

[20] Perau, E. W., Bearing Capacity of Shallow Foundations. Soils and Foundations, 37(4), 77-83, 1997.

[21] Okamura, M., Mihara, A., Takemura, J., Kuwano, J., Effects of Footing Size and Aspect Ratio on the Bearing Capacity of Sand Subjected to Eccentric Loading. Soils and Foundations, 42(4), 43-56, 2002.

[22] Janabi, F. H., Raja, R. A., Sakleshpur, V. A., Prezzi, M., Salgado, R., Experimental Study of Shape and Depth Factors and Deformations of Footings in Sand. Journal of Geotechnical and Geoenvironmental Engineering, 149(2), 04022128, 2023.

[23] Khezri, A., Moradi, M., Mir Mohammad Hosseini, S. M., Park, H., Lee, D., Effect of Footing Shape on the Rocking Behavior of Shallow Foundations. Buildings, 14(3), 573, 2024.

[24] Michalowski, R. L., Upper-Bound Load Estimates on Square and Rectangular Footings. Géotechnique, 51(9), 787-798, 2001.

[25] Zhu, M., Michalowski, R. L., Shape Factors for Limit Loads on Square and Rectangular Footings. Journal of Geotechnical and Geoenvironmental Engineering, 131(2), 223-231, 2005.

[26] Puzakov, V., Drescher, A., Michalowski, R. L., Shape Factor Sγ for Shallow Footings. Geomechanics and Engineering, 1(2), 113-120, 2009.

[27] Antão, A. N., da Silva, M. V., Guerra, N., Delgado, R., An Upper Bound-Based Solution for the Shape Factors of Bearing Capacity of Footings Under Drained Conditions Using a Parallelized Mixed F.E. Formulation With Quadratic Velocity Fields. Computers and Geotechnics, 41, 23-35, 103-120, 2012.

[28] Shafiqul Islam, M., Rokonuzzaman, M., Sakai, T., Shape Effect of Square and Circular Footing Under Vertical Loading: Experimental and Numerical Studies. International Journal of Geomechanics, 17(9), 06017014, 2017.

[29] Mohapatra, D., Kumar, J., Collapse Loads for Rectangular Foundations by Three-Dimensional Upper Bound Limit Analysis Using Radial Point Interpolation Method. International Journal for Numerical and Analytical Methods in Geomechanics, 43(2), 641-660, 2019.

[30] Mohapatra, D., Kumar, J., Bearing Capacity of Embedded Foundations Using Quasi-Kinematic Limit Analysis. Computers and Geotechnics, 117, 103275, 2020.

[31] Osman, A. S., Upper Bound Solutions for the Shape Factors of Smooth Rectangular Footings on Frictional Materials. Computers and Geotechnics, 115, 103177, 2019.

[32] Eurocode 7. Geotechnical Design – Part 1: General Rules, EN 1997-1:2004. 2004.

[33] Golder, H. Q., Fellenius, W., Kogler, F., Meischeider, H., Krey, H., Prandtl, L., The Ultimate Bearing Pressure of Rectangular Footings. Journal of the Institution of Civil Engineers, 17(2), 161-174, 1941.

[34] FHWA. Geotechnical Engineering Circular No. 6 Shallow Foundations. FHWA-SA-02–054. United States. Federal Highway Administration. Office of Bridge Technology, Washington, DC, USA. 2002.

[35] AASHTO. LRFD Bridge Design Specifications. American Association of State Highway and Transportation Officials, Washington, DC, USA. 2020.

[36] CFEM. Canadian Foundation Engineering Manual, 5th Ed., The Canadian Geotechnical Society, Canada. 2023.

[37] GEO. Foundation Design and Construction. GEO Publication No. 1/2006. The Government of the Hong Kong Special Administrative Region, Hong Kong. 2006.

[38] Yünkül, K., Usluoğulları, Ö. F., Gürbüz, A., Numerical Analysis of Geocell Reinforced Square Shallow Horizontal Plate Anchor. Geotechnical and Geological Engineering, 39(4), 3081-3099, 2021.

[39] Hakro, M. R., Kumar, A., Ali, M., Habib, A. F., de Azevedo, A. R., Fediuk, R., Sabri, M. M. S., Salmi, A., Awad, Y. A.., Numerical Analysis of Shallow Foundations with Varying Loading and Soil Conditions. Buildings, 12(5), 693, 2022.

[40] Alnmr, A., Alsirawan, R., Numerical Study of the Effect of the Shape and Area of Shallow Foundations on The Bearing Capacity of Sandy Soils. Acta Polytechnica Hungarica, 21(1), 103-120, 2024.

[41] Demirdöğen, S., Gürbüz, A., Yünkül, K., 3D-printed Geocells in Footing Systems: A Comprehensive Physical and Numerical Studies on Scaling and Performance under Centric and Eccentric Loading Scenarios. Transportation Geotechnics, 45, 101214, 2024.

[42] Örnek, M., Laman, M., Demir, A., Yıldız, A., Numerical Analysis of Circular Footings on Natural Clay Stabilized with a Granular Fill. Acta Geotechnica Slovenica, 9(1), 61-75, 2012.

[43] Demir, A., Yıldız, A., Laman, M., Örnek, M., Experimental and Numerical Analyses of Circular Footing on Geogrid-Reinforced Granular Fill Underlain by Soft Clay. Acta Geotechnica, 9, 711-723, 2014.

[44] Mansouri, M., Imani, M., Fahimifar, A., Ultimate Bearing Capacity of Rock Masses Under Square and Rectangular Footings. Computers and Geotechnics, 111, 1-9, 2019.

[45] Malik, Z. B., Alshameri, B., Jamil, S. M., Umar, D., Experimental and Numerical Modeling of Bearing Capacity of Foundations on Soft Clay Stabilized with Granular Material. International Journal of Geosynthetics and Ground Engineering, 7, 1-17, 2021.

[46] Gupta, S., Mital, A., A comparative study of bearing capacity of shallow footing under different loading conditions. Geomechanics and Geoengineering, 17(4), 1338-1349, 2022.

[47] Cerato, A. B., Lutenegger, A. J., Scale Effects of Shallow Foundation Bearing Capacity on Granular Material. Journal of Geotechnical and Geoenvironmental Engineering, 133(10), 1192-1202, 2007.

[48] Demirdöğen, S., Gürbüz, A., Yünkül, K., Performance of Eccentrically Loaded Strip Footings on Geocell-Reinforced Soil. Geotextiles and Geomembranes, 52(4), 421-434, 2024.

[49] Jaky, J., The Coefficient of Earth Pressure at Rest. Journal of the Society of Hungarian Architects and Engineers, 7, 355–358, 1944.

[50] Al-Defae, A. H., Caucis, K., Knappett, J. A., Aftershocks and the Whole-Life Seismic Performance of Granular Slopes. Géotechnique, 63(14), 1230-1244, 2013.

[51] Das, B. M., Shallow Foundations, 3rd ed., Boca Raton, USA. CRC press, 2017.

[52] Arı, A., Mısır, G., Three-Dimensional Numerical Analysis of Geocell Reinforced Shell Foundations. Geotextiles and Geomembranes, 49(4), 963-975, 2021.

[53] Kaya, Z., Erol, A., Comparison of Bearing Capacities of Undisturbed Organic Soils by Empirical Relations and 2D Finite Element Analysis. Arabian Journal of Geosciences, 14(19), 1975, 2021.

[54] Barari, A., Zhou, J., Bo Ibsen, L., Nazem, M., Nielsen, K., A Theoretical and Practical Framework Based on Plasticity Theory for the Drained Behavior of Single and Multiple Shallow Footings. International Journal for Numerical and Analytical Methods in Geomechanics, 47(16), 2872-2898, 2023.

[55] Budhu, M., Soil Mechanics and Foundations, 3rd ed., New York, USA. John Wiley and Sons, 2010.

[56] Coduto, D. P., Foundation Design: Principles and Practices, 2nd ed., USA. Pearson Education Limited, 2014.

[57] Bowles, J. E., Foundation Analysis and Design, 5th ed., New York, USA. McGraw-Hill Book Company, 1996.

[58] Fang, H. Y., Foundation Engineering Handbook, New York, USA. Springer Science and Business Media, 2013.

[59] Baban, T. M., Shallow Foundations: Discussions and Problem Solving, 1st ed., United Kingdom. John Wiley and Sons. 2016.

[60] Meigh, A. C., Nixon, I. K., Comparison of In Situ Tests for Granular Soils, 5th International Conference on Soil Mechanics and Foundation Engineering, Paris, France, 499-508, 1961.

[61] Rodin, S., Experiences with Penetrometers, with Particular Reference to the Standard Penetration Test, 5th International Conference on Soil Mechanics and Foundation Engineering, Paris, France, 517-521, 1961.

[62] Thorburn, S., Tentative Correction Chart for the Standard Penetration Test in Non-Cohesive Soils. Civil Engineering and Public Works Review, 58(683), 752-3, 1963.

[63] Aiban, S. A., Znidarčić, D., Centrifugal Modeling of Bearing Capacity of Shallow Foundations on Sands. Journal of Geotechnical Engineering, 121(10), 704-712, 1995.

[64] Adams, M. T., Collin, J. G., Large Model Spread Footing Load Tests on Geosynthetic Reinforced Soil Foundations. Journal of Geotechnical and Geoenvironmental Engineering, 123(1), 66-72, 1997.

[65] Mestat, P., Berthelon, J. Finite Element Modeling of Shallow Foundation Tests at the Labenne Site. Bull. Lab. Ponts Chaussees, 234, 37-67, 2001.

[66] Siddiquee, M. S. A., Tatsuoka, F., Tanaka, T., Tani, K., Yoshida, K., Morimoto, T., Model Tests and FEM Simulation of Some Factors Affecting the Bearing Capacity of a Footing on Sand. Soils and Foundations, 41(2), 53-76, 2001.

[67] Mosallanezhad, M., Hataf, N., Ghahramani, A., Experimental Study of Bearing Capacity of Granular Soils, Reinforced with Innovative Grid-Anchor System. Geotechnical and Geological Engineering, 26, 299-312, 2008.

[68] Ziccarelli, M., Valore, C., Muscolino, S. R., Fioravante, V., Centrifuge Tests on Strip Footings on Sand with a Weak Layer. Geotechnical Research, 4(1), 47-64, 2017.

[69] Kyparissis, A., Lopes, M. P., Bearing Capacity of Reinforced Soil under a Strip Footing: Centrifuge Tests. 11th International Conference on Geosynthetics, Seoul, Korea, 2018.

[70] Shadmand, A., Ghazavi, M., Ganjian, N., Scale Effects of Footings on Geocell Reinforced Sand Using Large-Scale Tests. Civil Engineering Journal, 4(3), 497-508, 2018.

[71] Wang, J. Q., Zhang, L. L., Xue, J. F., Tang, Y., Load-Settlement Response of Shallow Square Footings on Geogrid-Reinforced Sand Under Cyclic Loading. Geotextiles and Geomembranes, 46(5), 586-596, 2018.

[72] Bharti, G., Shukla, B. K., Srinivasan, V., Bansal, V., Experimental Study on Eccentrically Loaded Rectangular Footing on Sand for Embedded Condition to Enhance Serviceability of Structures. Materials Today: Proceedings, 61, 517-522, 2022.

[73] Latha, G. M., Venkateswarlu, H., Krishna, A., Geocell Anchor Cage for Enhanced Load Support in Soil Structures. Construction and Building Materials, 425, 135998, 2024.

[74] Hamed, E., Demiröz, A., Optimization of Geotechnical Characteristics of Clayey Soils Using Fly Ash and Granulated Blast Furnace Slag-Based Geopolymer. Construction and Building Materials, 441, 137488, 2024.

[75] Yünkül, K., Karaçor, F., Gürbüz, A., Budak, T. Ö., Prediction of the Undrained Shear Strength of Remolded Soil with Non-Linear Regression, Fuzzy Logic, and Artificial Neural Network. Journal of Mountain Science, 21(9), 3108-3122, 2024.

[76] Meyerhof, G. G., Influence of Roughness of Base and Ground-Water Conditions on the Ultimate Bearing Capacity of Foundations. Géotechnique, 5(3), 227–242, 1955.

[77] Cascone, E., Biondi, G., Casablanca, O., Groundwater Effect on Bearing Capacity of Shallow Strip Footings. Computers and Geotechnics, 139, 104417, 2021.

[78] Park, D., Kim, I., Kim, G., Lee, J., Groundwater Effect Factors for the Load-Carrying Behavior of Footings from Hydraulic Chamber Load Tests. Geotechnical Testing Journal, 40(3), 440-451, 2017.